Factors affecting printability of 316L powders using the DMLS process

Dmitri Riabov[1,*], Sven Bengtsson[2]
[1] Department of Industrial and Materials Science, Chalmers University of Technology, 412 96 Gothenburg, Sweden
[2] Höganäs AB, 263 83 Höganäs, Sweden

ABSTRACT: The layer by layer build-up of metal parts by selective laser melting puts specific requirements on the powder quality. The powder should be able to spread homogeneously throughout the layer, to melt and fuse without forming detrimental defects. Consequently, the clean, highly spherical gas atomized powders with excellent flowability are used in this process. However, little work has been published on water atomized powder since higher oxygen levels and lower apparent density can be expected and are believed to be detrimental to build quality. Several variants of water atomized powder was used to investigate the effects of higher levels of impurities and cohesivity on the properties of the built part. Powder properties were analyzed using traditional methods such as Hall flow, particle size distributions, and various density measurements in combination with a modern powder rheometer for characterization. The behavior during building was evaluated through metallographic investigations, mechanical properties and the chemistry of the printed parts. All of which were compared to the properties of built specimens with industry standard gas atomized powder and forged material. Results indicate that the experimental powders with poor flowability can be successfully spread out onto a bed and consolidated to full density when building with a small layer thickness. The resulting mechanical properties match closely the reference, except for significantly lower impact toughness. This is probably caused by increased numbers of spherical nano-sized oxides homogenously distributed in the structure. This is in turn caused by the higher oxygen contents in the experimental powder. It was also found that part integrity went down when increasing the build layer thickness for the experimental powders.
Key words:
stainless steel
316L
water atomized
DMLS
powder properties
mechanical properties

1. Introduction

The powder bed based AM processes, whether laser based or other means of powder consolidation, utilize highly spherical and high purity powders. The majority of these powders are produced through gas atomization, in which an inert gas, mostly argon or nitrogen, is used to break apart a liquid melt stream into droplets. The process yields relatively low solidification rates, thus allowing the disintegrated liquid droplets to spheriodize as they fall through the atomizing tower. The high sphericity enables these powder to easily flow and pack efficiently to high densities making them suitable for the powder bed fusion processes [1,2]. However, the final yield is usually low. The yield can be improved by optimizing the gas pressure, geometry of the atomizing nozzle and using close-couple atomization [3]. Although, gas atomization remains an expensive practice because of gas consumption and low productivity, especially when producing fine powders. In contrast, the cost for water atomized powder is significantly lower compared to gas atomization, a difference that increases for finer powder and with produced volumes.

There has been little research on the usage of water atomized powder in the powder bed fusion processes. Hoeges et al. [4] investigated water atomized 316L powders using a Renishaw M250 machine. The work focused on densification of built parts and mechanical evaluation. Results showed that it was possible to achieve 99.77% density using water atomized powders with mechanical properties slightly lower than those built with gas atomized powders. However, no details were given on which layer thickness was used nor did they investigate how the additive process affects oxygen content and distribution. In another study by Irrinki et al. [5] water atomized 17-4PH powder was compared to gas atomized powder. With the conclusions that water-atomized powder is able to match gas-atomized powders if the linear energy density of the laser beam was optimized. The study was mainly a parameter evaluation and the influence of such on mechanical properties,

*Corresponding author. MSc.
Email address: riabov@chalmers.se (D. Riabov)

almost no physical powder properties were provided and the chemistry was not analyzed. However, quite some research has been done on DMLS processed 316L using conventional powders [6–9]. Describing typical for the process elongated grains, with columnar dendrites growing in the direction of the heat flux. The mechanical properties are often surpassing cast and even forged materials – although elongation to fracture and impact toughness performing worse.

2. Experimental

Two different grades of commercially available 316L powder was acquired from Höganäs AB. The first grade was produced through nitrogen gas atomization, abbreviated as GA. The other grade was produced with water atomization, abbreviated WA. Grade GA was sieved at 20-53µm and WA was sieved at 25-63µm. Compositions of the two grades corresponded to nominal 316L chemistry, however, the WA grade had lower Mn concentration in order to minimize oxidation of Mn during atomization [10]. This is standard practice for powders used for sintering where oxidized particle surfaces are not tolerated. Grade WA was further modified using two different operations to improve the physical characteristics of the powder, and will be denominated as WA2 and WA3. Additional oxygen and particle size analysis were performed after the modifications of WA2 and WA3.

The composition of the powders was measured by using inductively coupled plasma optical emission spectroscopy (ICP-OES), except for lighter elements such as C, O, N and S which were analyzed through combustion gas analysis (LECO Corp., USA). Physical properties of the grades were measured through conventional methods; such as Hall-flow, apparent density, and tap density after 4000 taps. These were complimented with dynamic properties measured with a powder rheometer (Freeman FT4, Freeman Technology Ltd., UK). The Freeman FT4 outputs many properties, which will be briefly explained: Basic flowability energy (BFE) describes the total amount of resistance (torque and force) for the rotor to move through the powder in a downward motion, resembling confined flow. The specific energy (SE) is the unconfined flow as the rotor moves upward through the powder, resembling a powder layer recoating. Conditioned bulk density (CBD), is similar to apparent density however the rotor conditions the powder first by a downward counter-rotation followed by an upward rotation of the blade. The pressure drop (PD) describes how easily a stream of air could pass through the powder bed while applying a normal load of 15kPa. The compressibility of the powder bed was tested by measuring the travel of the cylinder at a normal load of 15kPa. A shear cell was also used to test the shear properties of the powder beds, the bed was first pre-compacted using a load of 9kPa and then sheared at varying normal loads. Based on this data yield loci were constructed and values such as cohesion, unconfined yield stress (UYS) and the flow function (FF) were calculated. The particle size distribution was measured by laser diffraction (Sympatec GmbH, Germany). The powder morphology and surfaces were investigated by a scanning electron microscope (Hitachi SU6600, Hitachi High-Technologies Europe GmbH, Germany).

Test coupons were built in an EOS M290 DMLS machine (EOS GmbH., Germany) using layer thicknesses of 20µm and 40µm, however only 20µm was utilized to build samples for mechanical evaluation. The 40µm thickness was used for evaluating porosity and the build process (such as re-coater blade strikes and excessive spatter generation) on 10x10x10mm^3 cubes, or printability in short. For the GA powder, a laser power of 195W and a scan speed of 1080 mm/s was utilized to build samples for impact (according to ISO 148-1, Charpy V-notch) and tensile (according to ISO 2740) testing. All of the specimens were oriented horizontally. 10x10x10mm^3 cubes were simultaneously built to verify successful builds with respect to porosity. For the WA powder process parameters had to be developed through design of experiments (DOE) in which laser power, scanning speed and hatching distance were varied and optimized for lowest residual porosity. Once optimal parameters were found, then the chosen parameter set was used to build samples for mechanical testing. Additional cubes were built in an EOS M100 machine to evaluate the printability of the modified powders, using layer thicknesses of 20, 30 and 40µm. A previously GA optimized parameter set for was used when printing with 20µm layers (107W, 830 mm/s). When printing with thicker layers, process parameters had to be developed using the same method as for the WA powder in the M290 machine. These were developed using the GA powder first and the optimal settings were used as starting points for the modified powders. The GA

and WA powders were also included for reference purposes, since EOS M100 has a smaller laser spot size thus influencing the laser intensity and possibly the melt pool characteristics.

The samples were cut from the build-plates and the support structures removed by machining. The samples were evaluated in both the as-built condition and in the stress relieved condition. No surface modifications were made. Stress relieving (according to AMS 2759)was done at 900°C for one hour followed by gas quenching using nitrogen at 200 kPa in a vacuum furnace by ECM (ECM Technologies, USA). The tensile tests were performed according to ISO 6892-1 in a Zwick Z100 tensile test machine (Zwick/Roell AG, Germany), 7 specimens were tested to get statistical representation. Impact tests were performed according to ISO 10045-1 in a pendulum impact tester (Instron Wolpert GmbH, Germany), 10 specimens were tested.

Test coupons for microstructural characterization were observed with a light optical microscope (Zeiss Axio Imager M2M, Carl Zeiss AG, Germany) and a scanning electron microscope. Samples were prepared by sectioning the 10x10x10mm^3 coupons roughly in the center, mounted in bakelite, ground and polished to get accurate pore representations. The density determinations were carried out in the as-polished condition, using the software imageJ. For microstructural and SEM investigations samples were electroetched in a solution of 10% oxalic acid in distilled water using a voltage of 3V until microstructures were revealed. A Bruker D8 Advance X-ray diffractometer with a Cr *Kα* source was used for phase identification and to detect preferential crystallographic orientations in built cubes.

3. Results

The measured chemical composition of the powders is displayed below in Table 1.

Table 1
Chemical composition of tested grades, Fe is balance (wt.%).

Powder	C	O	N	S	Si	Cr	Ni	Mn	Mo	Ti	Nb	Al	Ca	P
GA	0.01	0.07	0.14	0.01	0.70	16.6	12.4	1.5	2.5	0.001	0.01	0.02	0.01	0.02
WA	0.03	0.24	0.04	0.01	0.80	16.9	12.7	0.2	2.2	0.01	0.04	0.01	0.01	0.02

Table 2 shows the physical properties of the studied powders. The GA powder had higher flow, apparent and tap densities than WA. The WA powder showed slightly coarser size distribution than the GA powder, while WA2 and WA3 had a size distribution similar to GA. Thus, the large difference in packing efficiency and flow must be mostly due to morphological differences. The effects of the modifications on grades WA2 and WA3, could clearly be distinguished in increased flow and density values. The size distribution was also altered slightly in the modified versions, becoming narrower. Based on the oxygen analysis no oxidation had occurred during the operations.

Table 2
Physical properties of the tested powders, and measured oxygen content of the powders after the modification.

Powder	AD (g/cm^3)	TD (g/cm^3)	Flow (s/50g)	x_{10} (µm)	x_{50} (µm)	x_{90} (µm)	O (wt.%)
GA	4.3	4.9	18.1	26.1	42.2	63.3	0.07[1]
WA	2.4	3.1	37.4	25.8	46.5	70.4	0.24[1]
WA2	3.1	4.0	22.8	27.0	45.2	65.9	0.25[2]
WA3	3.7	4.6	16.4	24.9	41.0	58.8	0.23[2]

1) measured after atomization. 2) measured after modification

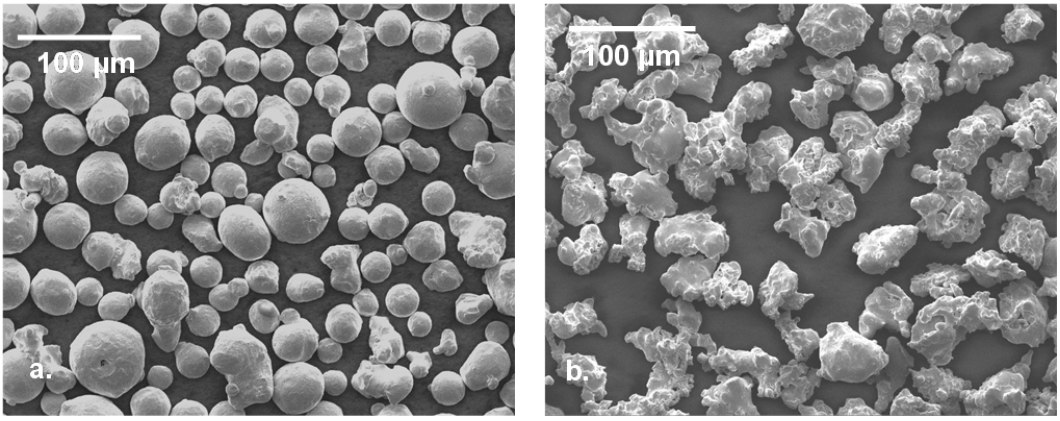
Table 3 shows the measurements from the Freeman FT4 powder rheometer. The total resistance for the rotor to plough downward through the powder bed (BFE), was the highest for the GA powder and lowest for the WA grade. BFE increased for the two modified grades. The scatter was observed to be larger for the water atomized grades than the gas atomized powder. Regarding the compressibility, the GA powder showed the lowest tendency to compress. WA and WA2 however, were able to compress 3%. Looking at the shear tests, the GA

powder had low values of cohesion and UYS and a high flow function, typical of a free flowing non-cohesive powder which correlated well with the flow values in Table 2. The WA powder on the contrary displayed higher cohesivity, again correlating well with values previously measured in Table 2. The modified powders showed a decrease in these properties – indicating a successful operation where small satellites and excessive roughness in the particles was removed or smoothed out. The WA3 powder displayed an anomaly since all measured shear values pointed toward an increase in cohesive properties even when Hall-flow was greater than the GA powder, the measured difference was small but consistent through additional measurements.

Table 3
Measured powder properties from the powder rheometer.

	Confined and unconfined flow		Bulk density		Compressibility	Shear tests		
Powder	BFE (mJ)	SE (mJ/g)	CBD ($g/cm^{3)}$	PD (mPa)	Mass at 15kPa (%)	Cohesion (kPa)	UYS (kPa)	FF
GA	599 ± 9	1.70	4.44	983	1.5 ± 0.02	0.04	0.11	108
WA	410 ± 16	2.35	2.63	341	3.1 ± 0.28	1.10	3.93	4
WA2	547 ± 19	2.73	3.15	610	3.0 ± 0.14	0.10	0.39	35
WA3	528 ± 15	2.16	3.89	1130	2.1 ± 0.09	0.15	0.46	28

SEM images of the powders are displayed in Fig. 1, as can be seen the powder GA was very typical for gas-atomized powders; highly spherical with low amount of satellites. The WA grade had a very irregular morphology with many features, typical for water atomized grades. This caused particle interlocking when subjected to flow and prevents efficient packing when settled in powder beds, seen by the measurements in Table 2 and Table 3. Based on the micrographs, the difference between WA and WA2 was very subtle. The modification of WA3 on the other hand completely altered the water-atomized morphology to a more spherical shape.



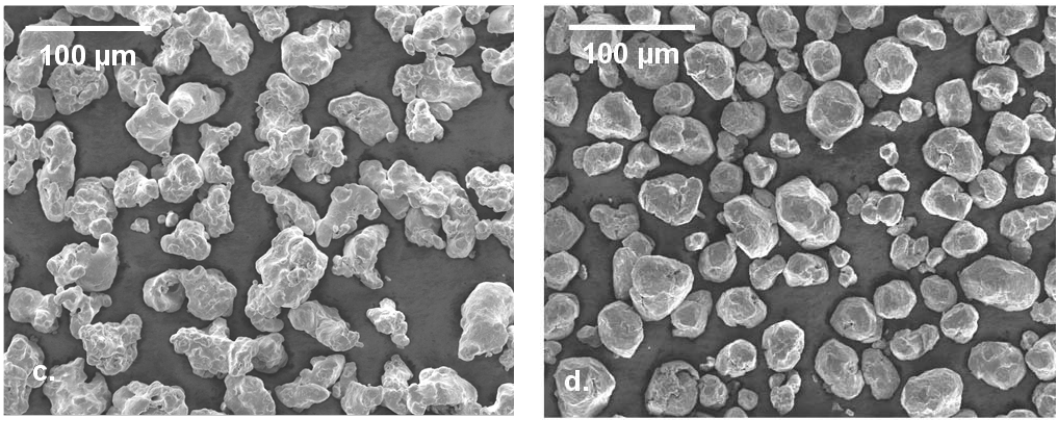
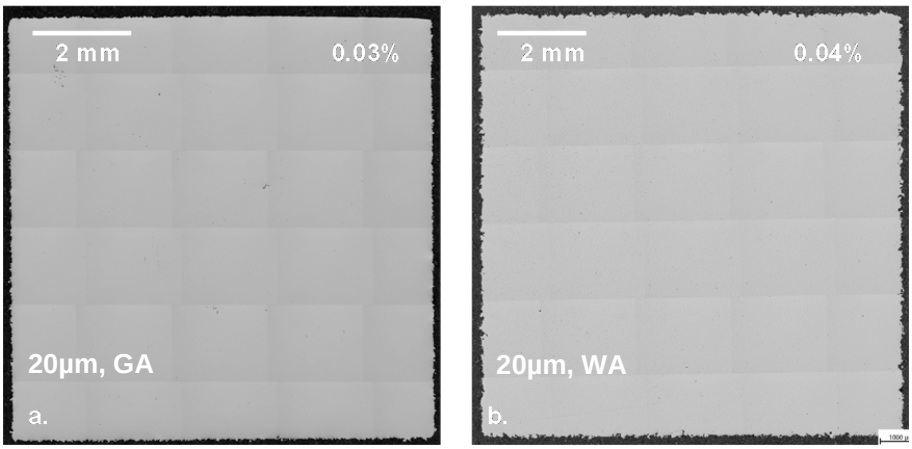


Fig. 1 SEM micrographs of the tested powders. a) GA. b) WA. c) WA2. d) WA3.

In Fig. 1 are cross sections perpendicular to the build direction of additively manufactured cubes built with the M290 machine using layers thicknesses of 20 and 40µm. No problems were encountered regarding the spreadability of the WA powder – layers were observed to be homogenous and without short feeding. For the 20µm layer build using the WA grade, after the initial DOE, parameters that gave the least amount of residual porosity were the parameters used for the GA powder. Therefore the same parameter set was used for both GA and WA grades during subsequent builds. Comparing the level of porosity with the gas atomized powder, the amount was almost on par differing only 0.01%. The resulting surface finish, although not measured, could be observed to have a more jagged appearance for the WA grade. No oxide films or stringers could be observed for the cube built with the WA powder, (see Fig. 2.) although some oxide inclusions averaging at 15µm were detected. In the builds using a layer thickness of 40µm differences between the powder grades GA and WA become more apparent as shown in Fig. 2. The GA powder had the highest density at a setting of 195W and a scan speed of 725 mm/s, while the settings for WA were; a laser power of 195W and a scan speed of 690mm/s. The cube built with the GA grade had a residual porosity of 0.06%, and the WA grade had a residual porosity of 0.95%. The melting process for the WA powder was observed to have some track instabilities resulting in balling, thus creating lack of fusion type defects during subsequent recoating and melting operations, see Fig. 2 d. Table 4 shows a chemical analysis of the built specimens with respect to C, O, N and S. Oxygen was observed to decrease for the water atomized grades, down to a level of 0.17wt.% from 0.24 wt.%.



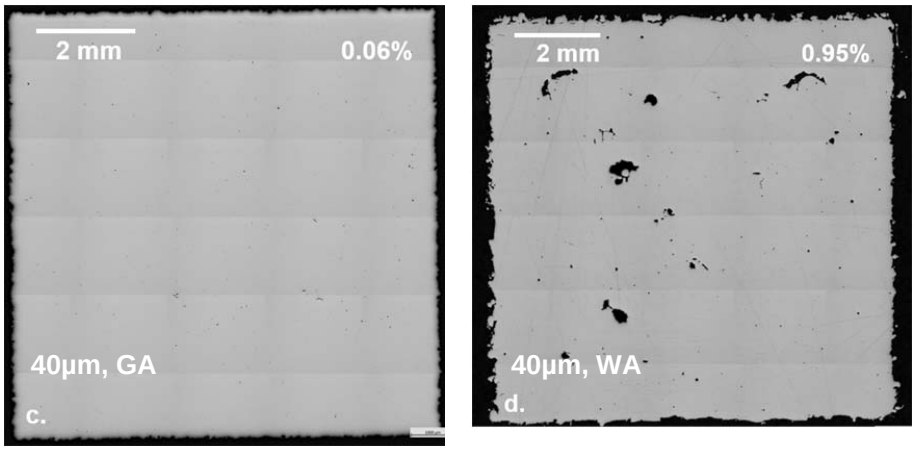


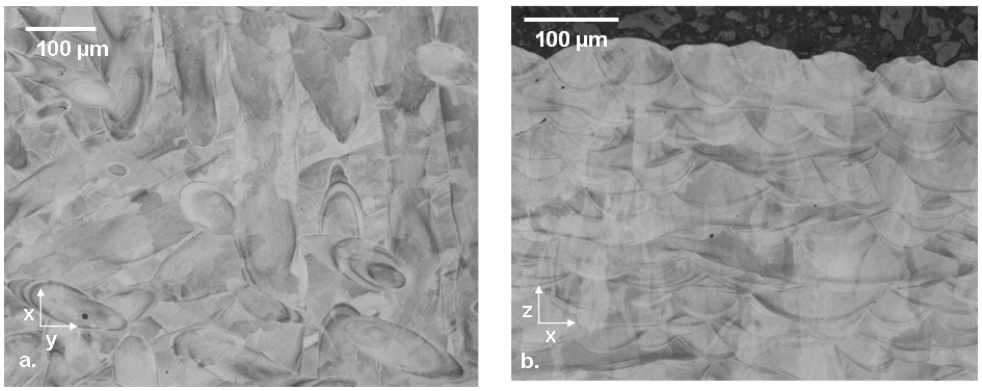
Fig. 2 LOM images of built cubes in the XY plane using layer thicknesses of 20 (a, b) and 40µm (c, d) in the M290 machine. a and c were made with the GA powder. b and d were made using the WA powder grade. Percentage of porosity indicated in right upper corners.

Table 4

Chemical analysis on built cubes given in weight percent.

Powder type and layer thickness	C	O	N	S
GA 20µm	0.03	0.05	0.13	0.008
WA 20µm	0.02	0.17	0.05	0.006
GA 40µm	0.03	0.07	0.34	0.007
WA 40µm	0.02	0.18	0.04	0.006

The etched microstructures of built cubes using a layer thickness of 20µm revealed completely austenitic structures without any delta ferrite stringers in both GA and WA grades, see Fig. 3. On a macro scale there were typical melt pool structures with a depth of up to 70µm. Grain morphology was elongated up to hundreds of microns along the build direction. On a micro scale the typical columnar dendrites were seen, however these were difficult to resolve with LOM, instead the SEM was used, see Fig. 4. No significant differences between the two powder grades could be detected, contrast variations were due to a slight variation of etching times.



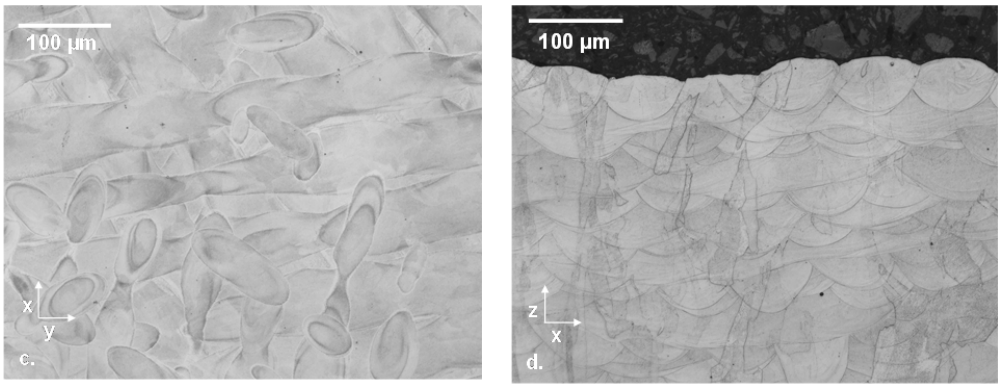


Fig. 3 LOM images of etched microstructures built using 20µm. a. b were made with GA powder. c. d were made with WA powder.

Scanning electron images revealed that both builds displayed similar columnar dendritic structure, with dendrites oriented in the heat-flux gradient. Fig. 4 shows the oxide distribution within the dendritic microstructure. Other than the larger particulates observed in the LOM images of the WA grade, spherical oxides under 1µm in size were homogenously distributed throughout the dendrites in both of the builds. Which could be seen by the jagged Swiss-cheese appearance of the dendrites. However, the number of particulates were greater in the WA powder, a closer examination would be required to fully quantify the population. Because of the small size of the particulates, EDX analysis could not be performed.

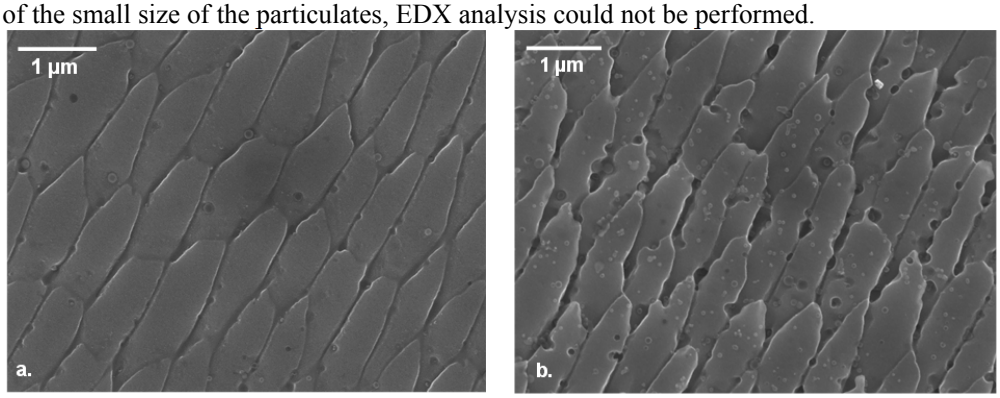


Fig. 4 SEM images of etched dendritic columnar structures. a. built with GA and b. built with WA.

Fig. 5 shows the XRD spectra of the powders, as-built cubes and stress-relieved cubes. Only the FCC phase was detected in all samples. Comparing the powder to the cubes, a preferred orientation was detected – common in additively manufactured components also indicated in Fig. 3 and 4. After stress-relieving the (220) peak was narrowed and intensified.

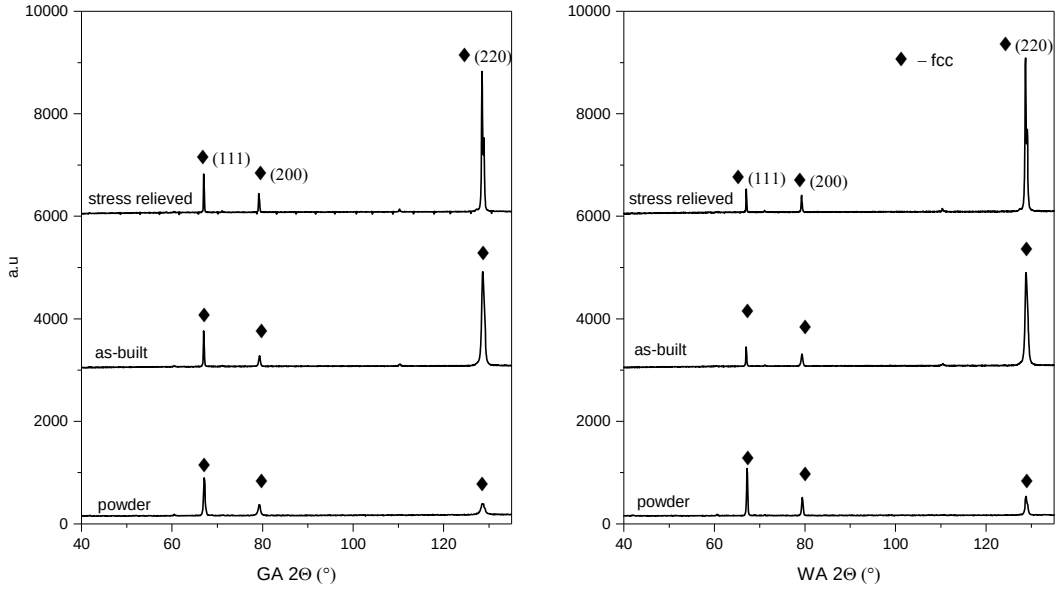


Fig. 5 XRD spectra for powders, as-built cubes and stress-relieved cubes. The horizontal plane of the cubes was analyzed.

Table 5 compares the mechanical properties of GA and WA samples built in the M290 machine, using a layer thickness of 20µm in the as-built and stress relieved condition. Reference values were provided by EN-10088, the standard for 316L cold-rolled sheet. In the as-built condition, most properties were within or exceeded the values stated in the standard, with elongation to fracture being lower. Comparing the two grades, WA had lower strength although elongation to fracture was similar to the GA powder. After the stress relieving heat treatment the values of YS and UTS were lowered for both grades, with elongation to fracture and impact toughness increasing. Possibly suggesting a reduction in the dislocation density within the samples. Impact toughness values were lower than its cast and forged counter parts, however this has been reported to be strongly dependent on the oxygen content of the sample [11–14].

Table 5
Mechanical data from test samples produced in the M290 machine using a layer thickness of 20 µm and compared to the EN-10088-2 standard for 316L cold-rolled sheet metal in the solution annealed condition.

Powder	0.2% YS (N/mm^2)	UTS (N/mm^2)	Elongation (%)	IE (J)	Hardness (GPa)
GA	601 ± 19	727 ± 3	28 ± 1	110 ± 3	2.20 ± 0.03
WA	504 ± 11	644 ± 5	27 ± 1	75 ± 1	1.86 ± 0.08
GA (stress relieved)	483 ± 30	678 ± 11	47 ± 1	134 ± 1	2.00 ± 0.06
WA (stress relieved)	435 ± 9	628 ± 9	44 ± 2	82 ± 2	1.75 ± 0.02
EN-10088-2	≥ 240	530-680	≥ 40	-	

Fig. 6 presents the porosity values of built cubes using the GA, WA, WA2 and WA3 powders with three different layer thicknesses in the M100 machine. Comparing with the results from the M290 machine drastically different results were noted when using the WA powder and a layer thickness of 20µm. Surfaces of the printed WA parts were rough, with valleys and mountains forming perpendicular to the re-coating direction. LOM images revealed a high fraction of porosity, with morphologies similar to the observed printed surfaces. The GA powder produced nearly identical results to the print in the M290 machine. However, the built parameters for the WA grades were not optimized. By altering the properties of the powder – increasing the

apparent density and the flow, could the porosity be reduced from 16% to 6% for WA2 and 0.1% for WA3 without changes in process parameters. Considering the 30 µm layer thickness a similar trend could be seen, but the porosity was lowered in the case of the WA2 powder since a prior optimization was performed. Optimal exposure parameters were: laser power of 170 W, scan speed of 800 mm/s and a hatch distance of 0.08 mm and gave the best results for all powder grades tested. The switch to 40 µm layer thickness resulted in increasing porosity levels for all of the water atomized grades while the GA grade had a residual porosity of 0.3%. Here, optimal settings varied and the WA powders benefitted from a faster scan speed compared to the gas atomized grade. The optimum for the GA powder: 170 W, 1000 mm/s and hatch distance of 0.06 mm while the WA powder was built with 1350 mm/s.

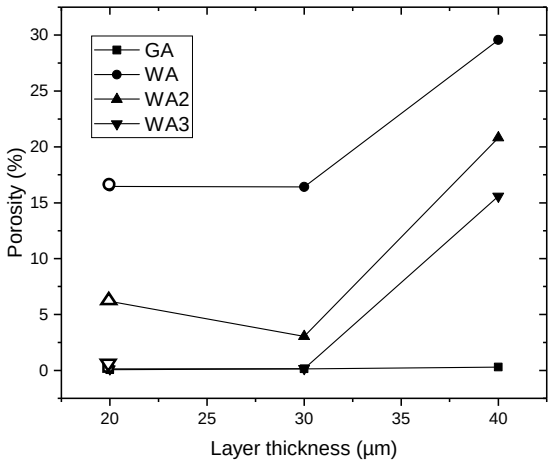


Fig. 6 Porosity of built cubes as a function of layer thickness on a M100 machine. Hollow symbols indicate that the parts were built using the GA powder parameters and solid symbols were built using parameters optimized for each powder grade and layer thickness.

4. Discussion

Within the powder-bed field the necessity for highly spherical powders is often mentioned, however details as to which property/-ies are the most important are vague. The two powders, GA and WA showed clearly different powder properties. The GA powder packed efficiently, had high flowability and negligible cohesive properties, while the WA grade exhibited the opposite trend. The two methods of measuring powder properties shown in Table 2 and Table 3 show some correlation. The CBD values resemble the apparent density and together with compressibility gives an indication how efficiently packed the powder is – if compressible then particles can rearrange more into a more favorable configurations. The shear tests correlate with Hall flow properties, and gives an indication of the flow characteristics. However, Hall-flow tests bulk flow as compared to the shear test which examines how particles interact under more constrained conditions. Based on the results from the builds, the flow characteristics did not seem to affect printability in a large extent. The rheometer outputs many values, which capture changes in powder behavior not necessarily captured by the standard methods, or extending the range of testing when e.g. powders are non-flowing. Such an example was found for WA3, BFE was decreasing while the bulk density was higher as compared to WA2 and the shear properties pointed toward a more shear resistant powder. Looking at the SEM images of the powders (see Fig. 4) could explain this behavior; the faceted shape of the particles of the WA3 powder could create a surface contact scenario rather than point contacts which would be occur for ideal spheres.

Laser beam characteristics were observed to have an effect on printability. Using process parameters optimized for the GA powder (varying between the two machines) porosity went from 0.04% when the laser spot size was 80 µm (M290 machine) to 16% when switching to a spot size of 40 µm (M100 machine). It is believed to be caused by the smaller spot irradiating a smaller area of the powder bed, and in the case of the water atomized

powder the bed could locally have large heterogeneities in terms of particle distribution. Thus creating melt track instabilities with resulting balling, residual porosity and lack of fusion. Bauereiß et al. [15] reported of defect networks similar to the ones found in this study when using the M100 machine. The proposed mechanism was that due to the stochastic nature of powder layers, a melt track would fuse heterogeneously under acting capillary forces. The subsequent layer enforces the heterogeneity through limited wetting to the previous layer – thus defect networks form. Similar findings were provided by Rausch et al. [16] however with the addition of varying powder bulk density in the simulations, concluding with that low density powder beds need more beam power to properly consolidate. This was however not found to be the case in this study. In other simulation efforts both stochastic powder layers and low packing densities gave rise to unstable melt dynamics resulting in porosity in the final solidified tracks [17,18]. However, all of the modeling effort was done using spherical particles.

Similar trend was observed when melting with a spot size of 80 µm but increasing the layer thickness. Although not as severe, it seems as the main contributing factor to defect generation is the degree of heterogeneity in the volume of powder as a function of the irradiated surface area. Another contributing factor is that the volume of powder which is irradiated scales with the bulk density of the powder bed, if bulk density is low then the effective powder layer thickness increases. If the laser spot size is small, and the powder is irregular with low packing density, then the layer thickness has to be scaled accordingly to retain full density. Also seen from the results when printing with the modified powders in the M100 machine, as the layer thickness increases the porosity increases too. As the effective powder layer (which can be up to 3 times thicker than the consolidated melt track) collapses during the laser interaction, it has to effectively de-gas and form a continuous track. During the "collapse" it has to not deviate from its intended location while being subjected to recoil pressure, Marangoni flow, surface tension and gravity [19–21]. Only by improving the packing efficiency of the powder could the porosity be reduced and match that of the gas atomized powder.

5. Conclusions

Printability using the water atomized grade with the M290 machine was good when using the GA optimized parameter set and a 20 µm layer thickness. The density and mechanical properties closely matching those when using the gas atomized powder.

The higher oxygen content in the powder did not seem to impact printability. But seems to have interacted with the laser beam and a fraction of it is believed to have been vaporized, since oxygen content in the built parts were lower as compared to the powder. The final oxygen content did not seem to be dependent on the layer thickness and reached a plateau at around 0.17 wt.% and was homogenously distributed as spherical oxides in the built material. The oxides are believed to be the source of the reduced impact toughness of the material.

The switch to the M100 machine reduced the printability for the WA powders, with the theory that the smaller irradiated area and thus the volume of the powder is behind this reduction.

Modifying the water atomized grade increased the packing density up to 54 % which improved printability and was comparable to the gas atomized grade in the M100 machine using layer thicknesses of 20 and 30 µm. The dominating powder property behind defect generation was believed to be the packing density and particle arrangement on a micro scale within the bed.

6. References

[1] C. Körner, Additive manufacturing of metallic components by selective electron beam melting — a review, Int. Mater. Rev. 61 (2016) 361–377. doi:10.1080/09506608.2016.1176289.

[2] J.H. Tan, W.L.E. Wong, K.W. Dalgarno, An overview of powder granulometry on feedstock and part performance in the selective laser melting process, Addit. Manuf. 18 (2017) 228–255. doi:10.1016/j.addma.2017.10.011.

[3] R. Ünal, Improvements to close coupled gas atomisation nozzle for fine powder production, Powder Metall. 50 (2007) 66–71. doi:10.1179/174329007X164899.
[4] S. Hoeges, A. Zwiren, C. Schade, Additive manufacturing using water atomized steel powders, Met. Powder Rep. 72 (2017) 111–117. doi:10.1016/j.mprp.2017.01.004.
[5] H. Irrinki, M. Dexter, B. Barmore, R. Enneti, S. Pasebani, S. Badwe, J. Stitzel, R. Malhotra, S.V. Atre, Effects of Powder Attributes and Laser Powder Bed Fusion (L-PBF) Process Conditions on the Densification and Mechanical Properties of 17-4 PH Stainless Steel, JOM. 68 (2016) 860–868. doi:10.1007/s11837-015-1770-4.
[6] Y.M. Wang, T. Voisin, J.T. McKeown, J. Ye, N.P. Calta, Z. Li, Z. Zeng, Y. Zhang, W. Chen, T.T. Roehling, R.T. Ott, M.K. Santala, P.J. Depond, M.J. Matthews, A.V. Hamza, T. Zhu, Additively manufactured hierarchical stainless steels with high strength and ductility, Nat. Mater. 17 (2017) 63–71. doi:10.1038/nmat5021.
[7] K. Saeidi, X. Gao, Y. Zhong, Z.J. Shen, Hardened austenite steel with columnar sub-grain structure formed by laser melting, Mater. Sci. Eng. A. 625 (2015) 221–229. doi:10.1016/j.msea.2014.12.018.
[8] W.M. Tucho, V.H. Lysne, H. Austbø, A. Sjolyst-Kverneland, V. Hansen, Investigation of effects of process parameters on microstructure and hardness of SLM manufactured SS316L, J. Alloys Compd. 740 (2018) 910–925. doi:10.1016/j.jallcom.2018.01.098.
[9] E. Liverani, S. Toschi, L. Ceschini, A. Fortunato, Effect of selective laser melting (SLM) process parameters on microstructure and mechanical properties of 316L austenitic stainless steel, J. Mater. Process. Technol. 249 (2017) 255–263. doi:10.1016/j.jmatprotec.2017.05.042.
[10] W. Schatt, E.P.M. Association, K.-P. Wieters, Powder metallurgy: processing and materials, European Powder Metallurgy Association, 1997.
[11] A. Lind, J. Sundström, A. Peacock, The effect of reduced oxygen content powder on the impact toughness of 316 steel powder joined to 316 steel by low temperature HIP, Fusion Eng. Des. 75–79 (2005) 979–983. doi:10.1016/j.fusengdes.2005.06.301.
[12] G.A. Rao, M. Srinivas, D.S. Sarma, Effect of oxygen content of powder on microstructure and mechanical properties of hot isostatically pressed superalloy Inconel 718, Mater. Sci. Eng. A. 435 (2006) 84–99. doi:10.1016/j.msea.2006.07.053.
[13] A.J. Cooper, N.I. Cooper, J. Dhers, A.H. Sherry, Effect of Oxygen Content Upon the Microstructural and Mechanical Properties of Type 316L Austenitic Stainless Steel Manufactured by Hot Isostatic Pressing, Metall. Mater. Trans. A. 47 (2016) 4467–4475. doi:10.1007/s11661-016-3612-6.
[14] Y. Nakayama, K. Kakehi, D. Kondo, Microstructure and Ductility of HIPed P/M 718 Using Thermal-Plasma-Droplet-Refined Powder, J. Jpn. Inst. Met. Mater. 78 (2014) 205–210. doi:10.2320/jinstmet.JBW201311.
[15] A. Bauereiß, T. Scharowsky, C. Körner, Defect generation and propagation mechanism during additive manufacturing by selective beam melting, J. Mater. Process. Technol. 214 (2014) 2522–2528. doi:10.1016/j.jmatprotec.2014.05.002.
[16] A.M. Rausch, V.E. Küng, C. Pobel, M. Markl, C. Körner, Predictive Simulation of Process Windows for Powder Bed Fusion Additive Manufacturing: Influence of the Powder Bulk Density, Materials. 10 (2017) 1117. doi:10.3390/ma10101117.
[17] Y. Lee, W. Zhang, Mesoscopic simulation of heat transfer and fluid flow in laser powder bed additive manufacturing, in: Proc. Annu. Int. Solid Free. Fabr. Symp. Austin TX USA, 2015: pp. 10–12.
[18] J. Zielinski, S. Vervoort, H.-W. Mindt, M. Megahed, Influence of Powder Bed Characteristics on Material Quality in Additive Manufacturing, BHM Berg- Hüttenmänn. Monatshefte. 162 (2017) 192–198. doi:10.1007/s00501-017-0592-9.
[19] S.A. Khairallah, A.T. Anderson, A. Rubenchik, W.E. King, Laser powder-bed fusion additive manufacturing: Physics of complex melt flow and formation mechanisms of pores, spatter, and denudation zones, Acta Mater. 108 (2016) 36–45. doi:10.1016/j.actamat.2016.02.014.
[20] P. Bidare, I. Bitharas, R.M. Ward, M.M. Attallah, A.J. Moore, Fluid and particle dynamics in laser powder bed fusion, Acta Mater. 142 (2018) 107–120. doi:10.1016/j.actamat.2017.09.051.
[21] S. Ly, A.M. Rubenchik, S.A. Khairallah, G. Guss, M.J. Matthews, Metal vapor micro-jet controls material redistribution in laser powder bed fusion additive manufacturing, Sci. Rep. 7 (2017) 4085. doi:10.1038/s41598-017-04237-z.